



Published in final edited form as:

Nat Methods. 2013 May ; 10(5): 407–409. doi:10.1038/nmeth.2413.

A bright monomeric green fluorescent protein derived from *Branchiostoma lanceolatum*

Nathan C. Shaner^{1,2,3}, Gerard G. Lambert¹, Andrew Chammas², Yuhui Ni², Paula J. Cranfill^{4,5}, Michelle A. Baird^{4,5}, Brittney R. Sell^{4,5}, John R. Allen^{4,5}, Richard N. Day⁶, Maria Israelsson⁷, Michael W. Davidson^{4,5}, and Jiwu Wang^{1,2}

Nathan C. Shaner: nathanshaner@scintillon.org

¹Department of Photobiology and Bioimaging, The Scintillon Institute, 6404 Nancy Ridge Dr., San Diego, CA 92121

²Allele Biotechnology and Pharmaceuticals, Inc., 6404 Nancy Ridge Dr., San Diego, CA 92121

³Author to whom correspondence should be addressed

⁴National High Magnetic Field Laboratory, 1800 E. Paul Dirac Dr., The Florida State University, Tallahassee, Florida 32310

⁵Department of Biological Science, 1800 E. Paul Dirac Dr., The Florida State University, Tallahassee, Florida 32310

⁶Department of Cellular & Integrative Physiology, Indiana University School of Medicine, 635 Barnhill Drive, MS 333, Indianapolis, IN 46202

⁷Department of Microbiology, Tumor and Cell Biology (MTC), Karolinska Institutet, Box 280, SE-171 77 Stockholm, Sweden

Abstract

Despite the existence of fluorescent proteins spanning the entire visual spectrum, the bulk of modern imaging experiments continue to rely on variants of the green fluorescent protein derived from *Aequorea victoria*. Meanwhile, a great deal of recent effort has been devoted to engineering and improving red fluorescent proteins, and relatively little attention has been given to green and yellow variants. Here we report a novel monomeric yellow-green fluorescent protein, mNeonGreen, which is derived from a tetrameric fluorescent protein from the cephalochordate

Users may view, print, copy, download and text and data- mine the content in such documents, for the purposes of academic research, subject always to the full Conditions of use: http://www.nature.com/authors/editorial_policies/license.html#terms

Author Contributions: M.I. cloned the original LanYFP gene from *Branchiostoma lanceolatum*, performed initial characterization of the protein, and identified the mutations I118K (dimerizing) and N174T (folding enhancement). G.G.L. performed the majority of library construction, *E. coli* expression experiments, and protein purification. A.C., J.W., and Y.N. performed initial cloning and library construction for screening dimeric variants. R.N.D. performed FLIM-FRET experiments. J.R.A. performed single-molecule superresolution imaging experiments. M.W.D., P.J.C., M.A.B., and B.R.S. constructed mammalian expression and fusion plasmids, performed fixed- and live-cell imaging and FRET experiments, and helped write the manuscript. J.W. contributed to writing and editing the manuscript and supported the project. N.C.S. designed and planned the project, performed library design and screening, optical characterization, and size exclusion experiments, and wrote the manuscript.

Competing Financial Interests: M.I. is affiliated with Innoventus (Uppsala, Sweden), which administers patent licensing for the original LanYFP clone. N.C.S., A.C., Y.N., and J.W. are affiliated with Allele Biotechnology and Pharmaceuticals, Inc., which holds an exclusive license to LanYFP from Innoventus. Allele has filed for patent protection of mNeonGreen. The Scintillon Institute is a non-profit research institute funded in part by Allele.

Branchiostoma lanceolatum. This fluorescent protein is the brightest monomeric green or yellow fluorescent protein yet described, performs exceptionally well as a fusion tag for traditional imaging as well as stochastic single-molecule superresolution imaging, and is an excellent FRET acceptor for the newest generation of cyan fluorescent proteins.

Since the initial cloning of *Aequorea victoria* green fluorescent protein (avGFP) over 20 years ago, fluorescent proteins have become staples of biological imaging. After an initial flurry of activity leading to the development of avGFP variants in the blue to yellow-green wavelength range¹, the bulk of subsequent fluorescent protein research has focused on expanding the fluorescent protein color palette into the red region and improving the brightness and performance of these longer-wavelength variants², along with more recent major improvements to cyan variants of avGFP (CFPs)³⁻⁵. Since green and yellow variants of the original avGFP (GFPs and YFPs) perform very reliably for most applications, a lesser degree of recent effort has been placed on developing novel fluorescent proteins in the green region of the spectrum. However, there is still room for improvement of green and yellow fluorescent proteins, both for routine imaging as well as more specialized applications such as Förster resonance energy transfer (FRET)^{6,7}.

Most newly-cloned green and yellow fluorescent proteins are not subjected to further engineering simply due to their lack of improved properties relative to existing GFPs. Thus, we were intrigued that a yellow fluorescent protein from *Branchiostoma lanceolatum* (LanYFP, Allele Biotechnology, San Diego, CA; GenBank Accession EU482389) exhibits an unusually high quantum yield (~ 0.95) and extinction coefficient ($\sim 150,000 \text{ M}^{-1}\text{cm}^{-1}$), making it a very attractive candidate for further development. Size exclusion chromatography revealed that, like the vast majority of naturally occurring fluorescent proteins, LanYFP is a tetramer (see Supplementary Fig. 1), and so we set out to monomerize it using a directed evolution approach that has proved highly successful for the development of many other fluorescent proteins⁸⁻¹⁰.

Guided by structural modeling of the wild-type LanYFP tetramer using I-TASSER and RosettaDock servers^{11,12}, we selected initial side chains for monomerization following the well-established approach of introducing positive charges at key interface positions, followed by structure-guided directed evolution to rescue fluorescence (see Supplementary Discussion, Supplementary Figs. 2-5, and Supplementary Data 1 and 2). The final mutant, designated mNeonGreen (GenBank Accession KC295282), contains a total of 21 mutations relative to tetrameric LanYFP (F15I, R25Q, A45D, Q56H, F67Y, K79V, S100V, F115A, I118K, V140R, T141S, M143K, L144T, D156K, T158S, S163N, Q168R, V171A, N174T, I185Y, F192Y), in addition to the appended EGFP-type termini⁹. Based on our models, these mutations are distributed over the A/B interface (I118K and N174T), the A/C interface (V140R, L144T, D156K, T158S, Q168R, and F192Y), additional external regions (R25Q, A45D, and S163N), and internal to the beta-barrel (F15I, Q56H, F67Y, K79V, S100V, F115A, T141S, M143K, V171A, and I185Y). We verified the monomeric status of mNeonGreen by size exclusion chromatography (see Supplementary Fig. 1). A sequence alignment of LanYFP, dLanYFP, and mNeonGreen can be found in Supplementary Fig. 6.

Our initial characterization of mNeonGreen revealed sharp excitation and emission peaks (506 nm and 517 nm, see Supplementary Fig. 7 and Table 1) somewhat blue-shifted relative to the original tetrameric LanYFP, placing it roughly midway between typical GFP and YFP wavelength classes. As such, it may be imaged with essentially no loss of emission photons using standard GFP bandpass or long pass filter sets, or separated from CFP signals with YFP filter sets with only minimal reduction in collection efficiency. mNeonGreen is also the brightest monomeric green or yellow fluorescent protein yet described. Its high quantum yield and extinction coefficient (see Table 1) make it between 1.5 and 3 times as bright as most commonly used GFPs and YFPs. Its photostability is slightly higher than that of mEGFP under widefield illumination (see Table 1 and Supplementary Fig. 8), but somewhat lower for laser illumination (~40% of mEGFP, see Supplementary Fig. 9), well within a practical range for most imaging applications. Its fluorescence pKa of ~5.7 is similar or superior to most modern GFPs and YFPs. mNeonGreen does not display any measurable sensitivity to Cl⁻ ions (data not shown). The oxygen-dependent maturation time of mNeonGreen was too short to measure using standard methods (see **Methods** and Supplementary Discussion), but based on our observations we estimated it to be < 10 minutes at 37 °C.

Subsequent to the completion of mNeonGreen engineering in this study, Clover, a novel bright yellow-green FP derived from avGFP, was independently reported⁷. Clover has very similar excitation and emission peak wavelengths to mNeonGreen and is nearly as bright, with slightly lower quantum yield and extinction coefficient. However, mNeonGreen has the notable advantages of superior photostability (~3-fold higher than Clover under both widefield and laser illumination), improved acid tolerance (mNeonGreen pKa of 5.7 versus 6.2 for Clover), and faster maturation (see Table 1). We additionally determined that mNeonGreen displays a substantially higher degree of monomeric character than Clover (see **Methods**, Supplementary Discussion, and Supplementary Table 1).

To determine the performance of mNeonGreen as a fluorescent probe in live cell imaging, we constructed fusion vectors to both the N and C terminus of the fluorescent protein. All fusions localized as expected, and mNeonGreen exhibited character typical of monomeric fluorescent proteins in “difficult” fusions, including histone H2B, connexins 26 and 43, and α -tubulin (see Figure 1 and Supplementary Figs. 10 and 11). Fusions of mNeonGreen with signal peptides and targeting proteins confirmed expected localization patterns in the cytoskeleton (β -actin, Lifeact, fascin, cortactin, plastin (fimbrin), MAP Tau, light chain myosin, myosin IIA, EB3, TPX2 and myotilin), intermediate filaments (keratin and vimentin), the Golgi complex (sialyltransferase, gal-T and mannosidase II), the nuclear envelope (lamin B1), nuclear pores (Nup50), nucleus (CAF1), endoplasmic reticulum (calnexin and calreticulin), the plasma membrane (annexin A4, CAAX, transferrin receptor, and C-src), nucleoli (fibrillarin), mitochondria (pyruvate dehydrogenase and TOMM20), endosomes (Rab4a, Rab5a, and RhoB GTPase), autophagosomes (LC3), centromeres (CENPB), tight junctions (β -catenin, VE-cadherin, and ZO1), DNA replication foci (PCNA), lysosomes (LAMP1), auto peroxisomes (peroxisomal membrane protein), various vesicles (clathrin and caveolin), and focal adhesions (α -actinin, talin, focal adhesion kinase, filamin A, VASP, paxillin, vinculin and zyxin). We observed all phases of mitosis in fusions

of human histone H2B to either the N or C terminus of mNeonGreen (see Supplementary Fig. 11).

Due to its high brightness and ability to be driven into a temporary dark state with high-power laser illumination, we reasoned that mNeonGreen would also be an excellent tag for single-molecule superresolution imaging of fusion proteins. We performed stochastic single-molecule superresolution imaging of zyxin, β -actin, keratin, and myosin IIA fusions to mNeonGreen, Clover, mEGFP, and mEmerald. In all cases, the performance of mNeonGreen in this mode of superresolution imaging was superior to all other FPs tested in terms of the number of molecules localized, the most critical metric of this imaging mode (on the order of 2-fold higher than Clover and 4-fold higher than mEGFP or mEmerald on average, see Supplementary Figs. 12, 13, 14, and 15). Because of its high extinction coefficient and quantum yield, we further expected that mNeonGreen would be a good FRET acceptor from cyan fluorescent proteins and a good FRET donor to red fluorescent proteins, as was recently demonstrated for the Clover-mRuby2 pair⁷. Most notably in our tests of FRET pairs, a direct fusion of mNeonGreen to mTurquoise⁵ achieved substantially higher FRET efficiency than identical constructs using mVenus¹³ or Clover as acceptors (see Supplementary Table 2). When used as a FRET donor to mRuby2, mNeonGreen achieved similar FRET efficiency to Clover in an otherwise identical construct (see Supplementary Table 2 and Supplementary Fig. 16). When measured using fluorescence lifetime imaging (FLIM, see **Methods**), the mTurquoise-mNeonGreen pair displays markedly higher FRET efficiency than the Clover-mRuby2 pair (32% versus 12%; data not shown). Moreover, for purposes of FLIM-FRET, mTurquoise is a superior donor due to its single-exponential fluorescence lifetime, versus the two-component fluorescence decay of Clover (and mNeonGreen), making the mTurquoise-mNeonGreen pair preferable to Clover-mRuby2 (Supplementary Table 3). Thus, we expect that mNeonGreen will be an excellent choice for a broad array of FRET applications.

As a representative of the evolutionarily distant cephalochordate fluorescent protein lineage¹⁴, LanYFP has low sequence identity to any fluorescent protein whose structure has been solved. However, modeling of its tetrameric configuration utilizing structure prediction and protein-protein docking algorithms provided sufficient information to identify the side chains to target for monomerization and to guide further directed evolution. The resulting monomeric variant, mNeonGreen, has optical properties which are superior to those of the most commonly used green and yellow fluorescent proteins, and is expected to be highly useful for general imaging, FRET probe design, and single-molecule superresolution imaging. Moreover, since it shares so little sequence identity with other commonly used fluorescent proteins, mNeonGreen will be an attractive target for antibody development, and should be amenable to orthogonal co-IP experiments along with jellyfish and coral-derived fluorescent proteins.

Online Methods

Modeling

The primary amino acid sequence of wild-type LanYFP (bIFP-Y3, GenBank accession ACA48232) was used as input to the I-TASSER structure prediction server¹¹ (<http://>

zhanglab.ccmb.med.umich.edu/I-TASSER/) using default parameters. The top-scoring structure returned by I-TASSER was aligned to the published tetramer crystal structure of dsFP483 (PDB ID 3CGL)¹⁷ to create two dimer configurations, which were designated “A/B” and “A/C” for the homologous DsRed dimer configurations^{8,18}. PDB files containing these starting dimer configurations were used as input to the RosettaDock server¹² (<http://rosettadock.graylab.jhu.edu/>) using default parameters. Several of the lowest energy configurations returned by the RosettaDock server for each dimer interface were used to identify the side chains most likely to be involved in critical dimer interactions. Alignment of predicted structures with existing crystal structures of related fluorescent proteins and generation of figures depicting structures was done using PyMol software (Schrödinger).

Cloning, protein expression, and purification

All fluorescent protein coding sequences were inserted between *Bam*HI and *Eco*RI sites in the constitutive expression vector pNCS which encodes an N-terminal 6×His tag and linker. Sequences for all primers used in this study are listed in Supplementary Table 4. Fluorescent proteins were expressed in *E. coli* strain NEBTurbo (New England Biolabs) or Mach1 (Invitrogen) by growing cultures in 2×YT medium supplemented with ampicillin overnight at 37 °C and shaking at 250 rpm. Fluorescent proteins were purified by Ni²⁺-affinity chromatography as previously described⁹. Proteins were eluted in 50 mM Tris pH 7.5 or 50 mM sodium phosphate buffer pH 7.5 containing 250 mM imidazole. For all further characterization experiments, eluted fluorescent proteins were buffer-exchanged using Amicon Ultra0.5 10 kD MWCO ultrafiltration units (Millipore) into the same buffer without imidazole. Proteins were found to be stable when stored at 4°C indefinitely or when frozen at –20 °C or –80 °C.

Directed evolution

Multiple rounds of directed evolution and screening were performed as previously described^{9,10}, with a summary of techniques following here. Screening of FP-expressing *E. coli* colonies was done by eye using a blue LED lamp and longpass yellow filter. For each round of directed evolution, one to three of the brightest clones from the previous round of were used as the template for construction of randomly mutagenized libraries using the GeneMorph II kit (Agilent Technologies). Mutagenic PCR conditions were chosen such that the library would contain an average of 2 to 4 mutations per clone. 20 to 30 of the brightest clones identified by random mutagenesis were sequenced, and any clones containing mutations predicted to revert the oligomeric state of the protein were rejected. The remaining amino acid positions identified by random mutagenesis were partially or fully randomized by directed mutagenesis by overlap extension PCR using degenerate primers, with library sizes typically between 500 and 25,000 unique clones. The brightest clones from directed mutagenesis were sequenced, optically characterized, and evaluated for their oligomeric state by size exclusion chromatography (see below). Those clones which possessed superior optical properties while maintaining the desired oligomeric state were used as the input for the next round of directed evolution.

Optical characterization

For spectroscopy measurements, all samples and buffers were filtered or centrifuged immediately before use. Purified fluorescent protein (FP) samples were diluted into 10 mM Tris, pH 7.4 buffer and fluorescein (Sigma) was diluted into 0.1 M NaOH. Absorbance measurements were collected with a Cary Bio 100 UV-Vis Spectrophotometer (Varian Inc.). Fluorescence measurements were collected with a Cary Eclipse Spectrophotometer (Varian Inc.). All measurements for absorbance were immediately preceded with a measured baseline with the appropriate blank buffer. Fluorescence pK_a values were determined by measuring fluorescence emission of heavily diluted (~ 10 nM) purified, dialyzed fluorescent protein samples in 100 mM mixed citrate-Tris-glycine buffer with pH ranging from 3 to 11.

Size Exclusion Chromatography

Purified and dialyzed fluorescent protein samples were diluted into 50 mM Tris-HCl pH 7.5, 100 mM NaCl and filtered through 0.2 μ m filters immediately prior to injection into a Shimadzu Nexera UHPLC equipped with a Waters BEH200 1.7 μ m 4.6×150 mm size exclusion column and 4.6×30 mm guard column. Samples were run in the same buffer at a flow rate of 0.3 ml per minute for a total run time of 20 minutes. Fluorescence of the eluted protein was detected with an RF-20Axs fluorescence detector (Shimadzu) with 480 nm and 540 nm excitation and 530 nm and 620 nm emission wavelengths. Each LanYFP or variant sample was co-injected with mCherry⁹, which had been purified under identical conditions and which served as a monomeric size standard. A control run of mCherry alone produced no bleedthrough into the yellow emission channel.

Quantum Yield (ϕ) and Extinction Coefficient (ϵ)

A sample of FP or fluorescein was prepared (typically at a concentration of approximately 5 μ M, giving a peak absorbance value of approximately 0.5) and its full absorbance spectrum was measured with 0.5 nm step size. This was done in the same cuvette to be used for fluorescence spectra measurement. Identically absorbing solutions (target OD = 0.05) were separately prepared in quadruplicate for the FP and fluorescein ($\phi = 0.925$)¹⁹ and their emission spectra were measured with 488 nm excitation. The excitation and emission bandwidths were 2.5 nm and 5 nm, respectively with 1.0 nm step size. Emission was collected for 490-750 nm and the integrated intensities for each sample were calculated using the fluorimeter's software. The average integrated intensities and their associated absorbance values were used to calculate quantum yields as previously described⁶.

Absorbance spectra of purified FP samples were measured in quadruplicate (0.5 nm step size) and were used to determine the mean peak absorbance value. A baseline absorbance spectrum was then measured with buffer diluted 1:1 with 2 M NaOH (1 M final concentration). A double-concentration sample was prepared in half the cuvette volume, mixed 1:1 with 2 M NaOH, and its absorbance was immediately measured. Data was acquired for NaOH-denatured protein between 430 and 460 nm (with a peak ~ 447 nm) and a full UV-Vis spectrum was measured for the last sample to ensure the protein fully denatured. Extinction coefficients were determined as described previously^{20,21} assuming that the denatured chromophore absorbed with an extinction coefficient equivalent to a denatured avGFP chromophore ($44,000 \text{ M}^{-1}\text{cm}^{-1}$).

Excitation and Emission

For excitation spectra, fluorescence emission was monitored at 535 nm. For emission spectra, fluorescence excitation was 465 nm with a 5.0 nm bandpass throughout.

Maturation

For oxygen-dependent maturation experiments, mNeonGreen was subcloned into a modified pBAD vector and grown as described⁹, with flasks sealed with parafilm after induction to exclude oxygen. Overnight cultures were observed under fluorescence excitation prior to unsealing to ensure that cultures remained non-fluorescent. After chilling on ice, flasks were unsealed, cultures were pelleted by centrifugation at 4 °C, and fluorescent protein was extracted by sonication on ice followed by clarification by centrifugation at 4 °C. This entire process following removal of the parafilm seal was streamlined to take under 20 minutes, and care was taken to minimize mixing and exposure to air prior to fluorescence measurements. Fluorescence emission from clarified lysates was taken at 5 minute intervals until the fluorescence signal reached a plateau, with samples incubated at 37 °C and open to the air between measurements.

Photobleaching

Laser-scanning confocal and widefield microscopy photobleaching experiments were performed as described previously^{2,10} utilizing fusions of the appropriate fluorescent protein to human histone H2B to allow for localized fluorescence in the nucleus. HeLa S3 cells were cultured in Dulbecco's modified Eagle's medium (DMEM; Invitrogen) supplemented with 12.5% fetal bovine serum (FBS; HyClone). The cells were then seeded onto 35 mm Delta T imaging dishes (Bioptechs) for live cell imaging. Approximately 24 hours after being seeded, cells were then transfected with 1 µg of DNA using Effectene (Qiagen) and maintained in a 5% CO₂ incubator for at least 24 hours before imaging.

Widefield photobleaching was performed on a Nikon TE2000 inverted microscope equipped with a Nikon Plan Fluorite 40× dry objective (NA = 0.85) and an X-Cite Exakte metal halide lamp (Lumen Dynamics). Photobleaching was conducted using a Brightline FITC-HYQ filter cube (Chroma) and a Newport 1918-C (Newport) optical power meter was used to verify that the illumination power at the objective was 4.3 mW. Power moderation was achieved by using neutral density filters contained within the lamp. With neutral density (ND32) in place, a region containing 10 to 20 evenly bright nuclei was located. The neutral density was then removed from the light path and the region was photobleached continuously with a 65ms exposure time for 15 minutes for a total of 4700 frames. Images were collected with a QImaging Retiga EXi camera (Photometrics, Tucson, AZ). Multiple regions were photobleached to ensure that data for 30 nuclei could be averaged. The raw data was collected using NIS-Elements software (Nikon) and then analyzed with Simple PCI software (Hamamatsu).

Confocal photobleaching measurements were collected on an Olympus FV1000 confocal microscope with an Olympus PLAPO 40× oil-immersion objective (NA = 1.0). A 488 nm Argon-ion laser line (Melles Griot) was confirmed to be attuned to an output power of 1005 µW at the objective with a FieldMax II-TO power meter (Coherent, Santa Clara, CA). The

microscope was set to a zoom of 2×, a pinhole size of 500 μm, a photomultiplier voltage of 450 V, an offset of 8, and a scan time of 4 μs/pixel. Emission was collected with detector slit settings of 505–605 nm. Utilizing an output of minimum laser power, a region of evenly bright nuclei was located. The laser power was raised back to 1005 μW and each region was photobleached continuously for ~8 minutes for a total of 300 frames, with multiple regions being bleached to ensure data for 30 nuclei. Raw data was collected with the FluoView software (Olympus) and then analyzed with Simple PCI software (Hamamatsu).

All photobleaching data were scaled to represent the equivalent of an emission rate of 1000 photons/s per fluorescent protein chromophore at time zero as previously described^{10,22}, a condition which produces a half-time of 150 s for mEGFP.

Acceptor Photobleaching FRET (AP FRET). FRET constructs of mTurquoise-mNeonGreen, mTurquoise-mVenus, mTurquoise-Clover, mCerulean-mVenus, mNeonGreen-mRuby2, and Clover-mRuby2 all contained a 10 amino acid linker –SGLRSPPVAT between FPs²³.

Acceptor photobleaching measurements were performed on an Olympus FV1000 confocal microscope with a UPLAPO 40× oil immersion objective (NA = 1.0), a Zeiss Elyra PS.1 inverted research microscope operated in laser scanning confocal mode with a PlanApo 63× oil immersion objective (NA=1.4) and a Zeiss LSM 5 Live with a PlanApo 63× oil immersion objective (NA=1.4). For measurements performed on the Olympus FV1000, a 515 nm Ar-ion laser line was used with a 458/515 dichroic mirror to excite and photobleach the mNeonGreen or mVenus in each FRET pair. Emission during acceptor photobleaching was collected in one channel spanning 528–553 nm to ensure bleaching of all fluorescence. For each of the CFP-YFP FRET constructs, a 405 nm diode laser line was used with a 405/488 dichroic for excitation of the CFP with one emission channel spanning 450–485 nm. The detector gain was set to 685 volts, the offset was set to 8 and the scan speed was set to 8.0 μs/pixel. Each experiment was performed with a pinhole size of 500 μm.

Measurements performed on the Zeiss Elyra PS.1 utilized a 561 nm Helium-Neon laser line used with a 488/561 dichroic mirror to excite and photobleach mRuby2 and a 514 nm Argon ion laser line to photobleach mNeonGreen or Clover in each FRET pair. Emission was collected in one channel spanning 568–638 nm for mRuby2 and 516–586 nm for mNeonGreen to ensure bleaching of all fluorescence. For CFP-YFP pairs, a 405 nm diode laser line was used with a 405 dichroic for excitation of the CFP with one emission channel spanning 436–488 nm. For YFP-RFP pairs, a 488 nm Argon ion laser line was used with a 488/561 dichroic for excitation of the YFP with one emission channel spanning 496–553 nm. The detector gain was set to 700, the zoom was 2.0, the scan speed was 1.6 μs/pixel, and the pinhole size was 600.9 μm for both FRET pairs. Measurements performed on the Zeiss LSM 5 Live utilized a 561 nm Helium-Neon laser line with a NFT565 beamsplitter paired with a bandpass filter BP575–615 to excite and photobleach mRuby2. The YFP donors were excited and imaged with a 489 nm Argon ion laser line paired with a R(405+532) beamsplitter and bandpass filter BP495–555.

For FRET efficiency measurements in live cells, a full view image of the donor was acquired before and after acceptor photobleaching of the entire cell. A region of interest (ROI) was drawn over identical areas of the cell in each image and the average intensities of these regions were calculated using the microscope's software. The following formula was

used to calculate the FRET efficiency of each construct: $FE = 1 - (\text{Average intensity donor PreAP} \div \text{Average intensity donor PostAP})^{23}$

For FRET efficiency measurements in fixed cells, a full view image of the donor was acquired before and after acceptor photobleaching. An ROI was drawn over an evenly bright part of the cell and acceptor photobleached. The average intensities of these regions were calculated using the microscope's software and the above FE formula was again used to calculate FRET efficiency.

Frequency domain fluorescence lifetime measurements (FD-FLIM)

The fluorescence lifetime measurements were made using a ISS ALBA FastFLIM system (ISS Inc.) coupled to an Olympus Ix71 microscope equipped with a 60× water-immersion objective lens (NA = 1.2). A stage top environmental control system (Pathology Devices Inc.) maintained temperature at 36 °C and CO₂ at 5%. A 5 mW 448 nm diode laser was modulated by the FastFLIM module of the ALBA system at the fundamental frequency of 20 MHz²⁴. The modulated laser is coupled to the ALBA scanning system, which is controlled by the VistaVision software (ISS Inc., Champaign, IL). The fluorescence signals emitted from the specimen are routed by a beam splitter through the 530/43 nm (acceptor emission) and the 480/40 nm (donor emission) band-pass emission filters. The signals are then detected using two identical avalanche photodiodes (APD). The phase delays and modulation ratios of the emission relative to the excitation are measured at seven modulation frequencies (20, 40, 60, 80, 100, 120, 140 MHz) for each pixel of an image.

The system is calibrated with the 50 μM Coumarin 6 dissolved in ethanol (lifetime 2.5 ns) to provide the software with a reference standard to estimate the lifetime values from the experimental data²⁴. Additionally, a second reference standard, 10 mM HPTS (8-hydroxypyrene-1,3,6-trisulfonic acid) dissolved in phosphate buffer (PB) pH 7.8 (lifetime of 5.4 ns) is used to check that the system is accurately reporting the fluorescence lifetime of a known sample. The distribution of the lifetimes for all the pixels in the image is determined using the phasor (polar) plot method^{25,26}. For live-cell imaging, transfected cells grown in chambered coverglass (2 well, Thermo Scientific) were identified by epifluorescence microscopy, and then imaged by FD-FLIM using the 448 nm laser line. The laser power was adjusted to achieve approximately 100,000 counts per second in the donor emission channel, and frame averaging was used to accumulate approximately 200 peak counts per pixel. The data were analyzed with the VistaVision software (ISS Inc.) using a region average for each selected square region of interest (ROI, typically 1-2 μm).

Fusion Plasmid Construction

mNeonGreen fluorescent protein expression vectors were constructed using C1 and N1 (Clontech-style) cloning vectors. The mNeonGreen cDNA was amplified with a 5' primer encoding an AgeI site and a 3' primer encoding either a BspEI (C1) or NotI (N1) site for generating cloning vectors to create C-terminal and N-terminal fusions (with regards to the FP), respectively. Purified and digested PCR products were ligated into similarly digested EGFP-C1 and EGFP-N1 cloning vector backbones. To obtain targeting fusion vectors, the appropriate cloning vector and a previously assembled EGFP or mEmerald fusion vector

were digested, either sequentially or doubly, with the appropriate enzymes and ligated together after gel purification.

Thus, to prepare mNeonGreen C-terminal fusions (number of linker amino acids in parenthesis), the following digests were performed: annexin A4 (12), NheI and BspEI (Alen Piljic, EMBL, Heidelberg, Germany; NM_001153.3); β -actin (7), NheI and BglII (human β -actin cDNA source: Clontech; NM_001101.3); β -catenin (20), XhoI and BamHI (mouse β -catenin cDNA source: Origene, Rockville, MD; NM_001165902.1); 20 amino acid farnesylation signal from c-Ha-Ras (CAAX; 5), AgeI and BspEI (c-Ha-Ras cDNA source: Clontech; NM_001130442.1); CAF1 (10), AgeI and BspEI (mouse chromatin assembly factor cDNA source: Akash Gunjan, Florida State University; NM_013733.3); caveolin 1 (10), NheI and BglII (human caveolin 1 cDNA source: Origene; NM_001753); endosomes (14), NheI and BspEI (endosomes cDNA source: Clontech; NM_004040.2); fascin (10), BspEI and BamHI (human fascin cDNA source: Origene; NM_003088.2); fibrillarin (7), AgeI and BspEI (fibrillarin cDNA source: Evrogen, Moscow, Russia; NM_001436.3); filamin A (14), BspEI and HindIII (human filamin cDNA source: David Calderwood, Yale University; NM_001456.3); human lysosomal membrane glycoprotein 1 (20), BamHI and NotI (LAMP1; George Patterson, NIH, Bethesda MD, U.S.A.; NM_012857.1); human light chain clathrin (15), NheI and BglII (human clathrin light chain cDNA source: George Patterson, NIH; NM_001834.2); human myotilin, AgeI and BspEI (MYOT; Origene; NM_006790.1); PCNA (19), AgeI and BspEI (proliferating cell nuclear antigen cDNA source: David Gilbert, FSU; NM_002592.2); plastin (10), BspEI and XhoI (human plastin 1 (fimbrin) cDNA source: Origene; NM_002670.1); canine Rab4a, BglII and BamHI (Rab4a cDNA source: Viki Allen, U. Manchester, UK; NM_004578.2); LC3B (7), AgeI and BspEI (rat LC3B cDNA source: Jenny M. Tam, Harvard University; U05784.1); talin (22) AgeI and BspEI (mouse talin 1 cDNA source: Clare Waterman, NIH; NM_011602.5); α -tubulin (18), NheI and BglII (human α -tubulin cDNA source: Clontech; NM_006082).

To prepare mNeonGreen N-terminal fusions (number of linker amino acids in parenthesis), the following digests were performed: human non-muscle α -actinin, EcoRI and NotI (cDNA source, Tom Keller, Florida State University (FSU), Tallahassee, FL, U.S.A.; NM_001130005.1); human calnexin, AgeI and NotI (Origene; NM_001746.3); c-src (7), BamHI and EcoRI (chicken c-src cDNA source: Marilyn Resh, Sloan-Kettering, New York; XM_001232484.1); connexin-43 (7), BamHI and NotI (rat Cx43 cDNA source: Matthias Falk, Lehigh U; NM_001004099.1); EB3 (7), BglII and BamHI (EB3 cDNA source: Lynne Cassimeris, Lehigh University; NM_012326.2); human keratin 18, EcoRI and NotI (Open Biosystems; NM_199187.1); lamin B1 (10), EcoRI and BamHI (human lamin B1 cDNA source: George Patterson, NIH; NM_005573.2); Lifeact (7), BamHI and NotI (Lifeact cDNA source: IDT); mouse mannosidase 2 (112 N-terminal amino acids, MANNII; 10), NheI and BamHI (cDNA source: Jennifer Lippincott-Schwartz, NIH; NM_008549.2); myosin IIA (14) NheI and BglII (mouse myosin IIA cDNA source: Origene; NM_022410.2); human nucleoporin 50kDa, BamHI and NotI (NUP50 cDNA source: Origene; NM_007172.2); human pyruvate dehydrogenase, AgeI and NotI (human PDHA1 cDNA source: Origene; NM_000284); human peroxisomal membrane protein, NotI and AgeI (PMP cDNA source: Origene; NM_018663.1); human MAP Tau (10), AgeI and NotI (MAP Tau cDNA source: Origene; NM_016841); human TfR (20), BamHI and NotI

(transferrin receptor cDNA source: George Patterson, NIH; NM_NM_003234); human TPX2 (10), AgeI and NotI (TPX2 cDNA source: Patricia Wadsworth, University of Massachusetts, Amherst; NM_012112.4); mouse VASP (10), NheI and BamHI (cDNA source: Clare Waterman, NIH; NM_009499); vascular epithelial cadherin (10), AgeI and NotI (human VE cadherin cDNA source: Origene; NM_001795.3), vimentin (7), BamHI and NotI (human vimentin cDNA source: Robert Goldman, Northwestern University; NM_003380.3), zyxin (6), BamHI and NotI (human zyxin cDNA source: Origene; NM_003461). All DNA for transfection was prepared using the Plasmid Maxi kit (QIAGEN). To ensure proper localization, mNeonGreen fusion proteins were characterized by transfection in HeLa (S3 or CCL2 line) or MDCK cells (ATCC) using Effectene (QIAGEN) and ~1 µg vector. Transfected cells were grown on coverslips in DMEM/F12, fixed after 48 hours, and mounted with Gelvatol. Epifluorescence images were captured with a Nikon 80i microscope using widefield illumination and a Chroma FITC filter set to confirm proper localization.

Microscopy

All filters for fluorescence screening and imaging were purchased from Chroma Technology, Omega Filters, or Semrock, Inc.. HeLa epithelial (CCL-2, ATCC) and grey fox lung fibroblast (CCL-168, ATCC) cells were grown in a 50:50 mixture of DMEM (Dulbecco's modified Eagle's medium) and Ham's F12 with 12.5% Cosmic calf serum (Thermo Scientific) and transfected with Effectene (QIAGEN). Imaging was performed in Delta-T culture chambers (Bioptechs) under a humidified atmosphere of 5% CO₂ in air. Imaging in widefield mode was performed with a Nikon (Melville, NY) TE-2000 inverted microscope equipped with Omega QuantaMax™ filters and a Photometrics Cascade II camera or an Olympus IX71 inverted microscope equipped with Semrock BrightLine™ filters and a Hamamatsu ImagEM™ camera. Laser-scanning confocal microscopy was conducted using a Nikon C1Si and an Olympus FV1000, both equipped with argon-ion (457 and 488 nm) and helium-neon or diode (543 and 561 nm respectively) lasers and proprietary filter sets. Spinning disk confocal microscopy was performed on an Olympus DSUIX81 equipped with a Lumen 200 illuminator (Prior Scientific), a Hamamatsu 9100-13 EMCCD camera, Semrock filters and ten-position filter wheels driven by a Lambda 10-3 controller (Sutter). In some cases, cell cultures expressing fluorescent protein fusions were fixed after imaging in 2% (w/v) paraformaldehyde (Electron Microscopy Sciences) and washed several times in PBS containing 0.05 M glycine before mounting with a polyvinyl alcohol-based medium.

Superresolution Imaging Sample Preparation

HeLa CCL-2 or S₃ (ATCC) cells were seeded and grown in 35 mm glass-bottom dishes (MatTek Corporation) to approximately 80% confluency. The culture medium was a 1:1 mixture of DMEM (Dulbecco's modified Eagle's medium) and Ham's F-12, supplemented with 12.5% Cosmic calf serum (Thermo Scientific). Cells were transiently transfected with plasmids coding for one of four fluorescent proteins (mNeonGreen, Clover, mEGFP, or mEmerald) fused to actin, zyxin, keratin, or myosin IIA using Effectene (QIAGEN). At ~24 hours post-transfection, cells were fixed using 2% (w/v) paraformaldehyde (Electron

Microscopy Sciences) for 15 minutes or, for keratin constructs, with cold methanol for 10 minutes. Live-cell imaging was conducted on selected cultures.

Stochastic Single-molecule Superresolution (SSMS) Imaging

Imaging was performed on a Zeiss Elyra PS.1 inverted research microscope operated in total internal reflection fluorescence (TIRF) illumination mode using a Zeiss PlanApo 63x oil immersion objective (NA = 1.4) with a 1.6 optovar placed in the light path, and a detection window of 495-575 nm. All images were collected over a $40.48 \times 40.48 \mu\text{m}$ area of an electron-multiplying CCD camera (EMCCD; Andor iXon DU 897) with a frame size of 256×256 . Fluorescent proteins screened for SSMS imaging performance in this study were imaged using a 488 nm diode laser line, with initial powers ranging from 15.1-31.9 mW/cm² to drive the majority of the molecules into a dark state, followed by the imaging of single emitters at lower intensities of approximately 3.05-6.08 mW/cm² for the remainder of each experiment. Laser power was measured at the objective. 5000 frames of data were collected for imaging experiments with zyxin and actin constructs, 10000 frames for myosin IIA, and 15,000 frames for keratin constructs. Data was collected at a frame rate of 10 Hz with a camera gain value of 250. Live cell imaging was performed in the original growth medium. Fixed actin and zyxin constructs were imaged in a 1% polyvinyl alcohol/PBS solution, while fixed keratin and myosin IIA constructs were imaged in 10 mM cysteamine in PBS.

Data Analysis

SSMS imaging datasets were analyzed using the PALM analysis module available in the Zen 2010D software (Zeiss). The detection parameters for single emitters were kept constant across all experiments, with a peak mask size of 9 pixels and a minimum peak intensity to noise ratio of 6.0. Data from all overlapping emitters was discarded and molecules were localized using a 2D Gaussian fit. Following initial analysis, model-based drift correction was applied and single molecules emitting across multiple frames were grouped together. Grouping of molecules followed strict parameters, with a maximum on-time of 5 frames, a fluorescence off-gap of 0 frames, and a capture radius of 1 pixel. Molecules emitting in excess of 5000 photons were filtered in order to prevent confusion with possible fluorescent artifacts or fiducial markers. All data were restricted to single molecules emitting between 150 and 1200 photons for statistical analysis to exclude outliers.

OSER Live Cell Assay

To anchor the fluorescent protein to the cytosolic face of the ER, the first 29 amino acids of Rabbit Cytochrome p450 (CytERM) were inserted into a mEGFP-N1 (Clontech-style) vector as previously described^{27,28}. All FP-CytERM fusions contained a 17 amino acid linker (RILQSTVPRARDPPVAT) between the fluorescent protein and CytERM signaling peptide sequence. Using AgeI and NotI sites, EGFP, mEGFP, mNeonGreen, Clover, mTurquoise and mRuby2 were inserted downstream of the p450 transmembrane segment. HeLa (CCL-2, ATCC) cells were cultured in Dulbecco's modified Eagle's medium (DMEM; Invitrogen) supplemented with 12.5% fetal bovine serum (FBS; HyClone). The cells were then seeded onto 35 mm culture dishes containing 18×18 mm glass coverslips. Approximately 24 hours after being seeded, cells were then transfected with 1 μg of DNA using Effectene (Qiagen) and maintained in a 5% CO₂ incubator for at least 24 hours before

counting. Transient transfections were visually assayed on an Olympus IX71 inverted microscope equipped with an LCPlanFluor 40x dry objective (NA = 0.60) and the appropriate filter sets. Cell counting was performed by counting the total number of cells within a viewfield and then counting the number of cells that had normally expressing ER. A cell was considered to be normally expressing if it contained no artifacts resembling organized smooth ER structures (e.g. stacked cisternae or “whorls”). Multiple viewfields were counted for several transfected dishes until a total of 10,000 cells had been counted. The number of normally expressing cells was divided by the total number of cells to determine a percentage of properly expressing cells for each protein fusion.

Supplementary Material

Refer to Web version on PubMed Central for supplementary material.

Acknowledgments

We thank S.H. Haddock (Monterey Bay Aquarium Research Institute) for the use of his lab's Shimadzu UHPLC instrument and W.R. Francis for help in compiling data, and S.G. Gilbert, J.D. Allen, C. Malik, and R.A. Evans for their helpful contributions.

Reference List

1. Tsien RY. The green fluorescent protein. *Annu Rev Biochem.* 1998; 67:509–544. [PubMed: 9759496]
2. Shaner NC, Patterson GH, Davidson MW. Advances in fluorescent protein technology. *J Cell Sci.* 2007; 120:4247–4260. [PubMed: 18057027]
3. Goedhart J, et al. Structure-guided evolution of cyan fluorescent proteins towards a quantum yield of 93%. *Nat Comms.* 2012; 3:751.
4. Markwardt ML, et al. An Improved Cerulean Fluorescent Protein with Enhanced Brightness and Reduced Reversible Photoswitching. *PLoS ONE.* 2011; 6:e17896. [PubMed: 21479270]
5. Goedhart J, et al. Bright cyan fluorescent protein variants identified by fluorescence lifetime screening. *Nature Methods.* 2010; 7:137–139. [PubMed: 20081836]
6. Miyawaki A. Development of probes for cellular functions using fluorescent proteins and fluorescence resonance energy transfer. *Annu Rev Biochem.* 2011; 80:357–373. [PubMed: 21529159]
7. Lam AJ, et al. Improving FRET dynamic range with bright green and red fluorescent proteins. *Nature Methods.* 2012; 9:1005–1012. [PubMed: 22961245]
8. Campbell RE, et al. A monomeric red fluorescent protein. *Proc Natl Acad Sci USA.* 2002; 99:7877–7882. [PubMed: 12060735]
9. Shaner NC, et al. Improved monomeric red, orange and yellow fluorescent proteins derived from *Discosoma* sp. red fluorescent protein. *Nat Biotechnol.* 2004; 22:1567–1572. [PubMed: 15558047]
10. Shaner NC, et al. Improving the photostability of bright monomeric orange and red fluorescent proteins. *Nature Methods.* 2008; 5:545–551. [PubMed: 18454154]
11. Roy A, Kucukural A, Zhang Y. I-TASSER: a unified platform for automated protein structure and function prediction. *Nature Protocols.* 2010; 5:725–738. [PubMed: 20360767]
12. Lyskov S, Gray JJ. The RosettaDock server for local protein-protein docking. *Nucleic Acids Res.* 2008; 36:W233–8. [PubMed: 18442991]
13. Nagai T, et al. A variant of yellow fluorescent protein with fast and efficient maturation for cell-biological applications. *Nat Biotechnol.* 2002; 20:87–90. [PubMed: 11753368]
14. Li G, Zhang QJ, Zhong J, Wang YQ. Evolutionary and functional diversity of green fluorescent proteins in cephalochordates. *Gene.* 2009; 446:41–49. [PubMed: 19615432]

15. Ai HW, Olenych SG, Wong P, Davidson MW, Campbell RE. Hue-shifted monomeric variants of *Clavularia* cyan fluorescent protein: identification of the molecular determinants of color and applications in fluorescence imaging. *BMC Biol.* 2008; 6:13. [PubMed: 18325109]
16. Karasawa S, Araki T, Yamamoto-Hino M, Miyawaki A. A green-emitting fluorescent protein from *Galaxeidae* coral and its monomeric version for use in fluorescent labeling. *J Biol Chem.* 2003; 278:34167–34171. [PubMed: 12819206]
17. Malo GD, et al. Crystal structure and Raman studies of dsFP483, a cyan fluorescent protein from *Discosoma striata*. *J Mol Biol.* 2008; 378:871–886. [PubMed: 18395223]
18. Yarbrough D, Wachter RM, Kallio K, Matz MV, Remington SJ. Refined crystal structure of DsRed, a red fluorescent protein from coral, at 2.0-Å resolution. *Proc Natl Acad Sci USA.* 2001; 98:462–467. [PubMed: 11209050]
19. Magde D, Wong R, Seybold PG. Fluorescence quantum yields and their relation to lifetimes of rhodamine 6G and fluorescein in nine solvents: improved absolute standards for quantum yields. *Photochemistry and Photobiology.* 2002; 75:327–334. [PubMed: 12003120]
20. Gross LA, Baird GS, Hoffman RC, Baldrige KK, Tsien RY. The structure of the chromophore within DsRed, a red fluorescent protein from coral. *Proc Natl Acad Sci USA.* 2000; 97:11990–11995. [PubMed: 11050230]
21. Chalfie, M.; Kain, SR. *Green Fluorescent Protein: Properties, Applications, and Protocols.* Wiley-Interscience; 2006.
22. Shaner NC, Steinbach PA, Tsien RY. A guide to choosing fluorescent proteins. *Nature Methods.* 2005; 2:905–909. [PubMed: 16299475]
23. Subach OM, Cranfill PJ, Davidson MW, Verkhusha VV. An Enhanced Monomeric Blue Fluorescent Protein with the High Chemical Stability of the Chromophore. *PLoS ONE.* 2011; 6:e28674. [PubMed: 22174863]
24. Sun Y, Day RN, Periasamy A. Investigating protein-protein interactions in living cells using fluorescence lifetime imaging microscopy. *Nature Protocols.* 2011; 6:1324–1340. [PubMed: 21886099]
25. Colyer RA, Lee C, Gratton E. A novel fluorescence lifetime imaging system that optimizes photon efficiency. *Microsc Res Tech.* 2008; 71:201–213. [PubMed: 18008362]
26. Redford GI, Clegg RM. Polar plot representation for frequency-domain analysis of fluorescence lifetimes. *J Fluoresc.* 2005; 15:805–815. [PubMed: 16341800]
27. Snapp EL, et al. Formation of stacked ER cisternae by low affinity protein interactions. *The Journal of Cell Biology.* 2003; 163:257–269. [PubMed: 14581454]
28. Costantini LM, Fossati M, Francolini M, Snapp EL. Assessing the tendency of fluorescent proteins to oligomerize under physiologic conditions. *Traffic.* 2012; 13:643–649. [PubMed: 22289035]

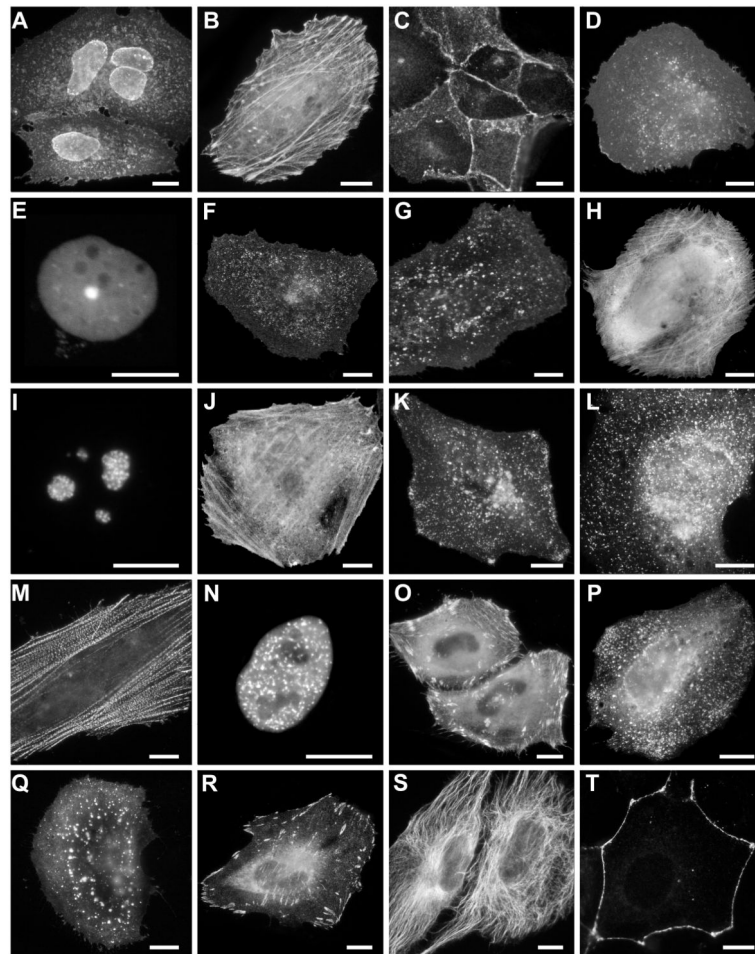


Figure 1.

Fluorescence imaging of mNeonGreen (mNG) fusion vectors. C-terminal mNG fusion constructs (with respect to the fluorescent protein); for each fusion, the linker amino acid length is indicated after the name of the targeted organelle or fusion partner: **(a)** mNG-Annexin (A4)-C-12 (human; plasma membrane); **(b)** mNG- β -actin-C-18 (human; actin cytoskeleton); **(c)** mNG- β -Catenin-C-20 (mouse; tight junctions); **(d)** mNG-CAAX-C-5 (20-amino acid farnesylation signal from c-Ha-Ras; plasma membrane); **(e)** mNG-CAF1-C-10 (mouse chromatin assembly factor); **(f)** mNG-Caveolin1-C-10 (human); **(g)** mNG-Endosomes-C-14 (human RhoB GTPase); **(h)** mNG-Fascin-C-10 (human; actin bundling); **(i)** mNG-Fibrillarin-C-7 (human; nucleoli); **(j)** mNG-FilaminA-C-14 (human; cytoskeleton); **(k)** mNG-LAMP1-C-20 (rat; lysosomal membrane glycoprotein 1; lysosomes); **(l)** mNG-Clathrin-C-15 (human, light chain B); **(m)** mNG-Myotilin-C-14 (human; actin filaments); **(n)** mNG-PCNA-C-19 (human; replication foci); **(o)** mNG-Plastin-C-10 (human; actin binding); **(p)** mNG-Rab4a-C-7 (human; endosomes); **(q)** mNG-LC3B-C-7 (rat light chain; autophagosomes); **(r)** mNG-Talin-C-18 (mouse; focal adhesions); **(s)** mNG-Tubulin-C-35 (human; microtubules); **(t)** mNG-ZO1-C-14 (human; tight junctions). The cell line used for expression of C-terminal mNG constructs was Madin-Darby canine kidney (MDCK; ATCC,

CCL-34) cells in panels (c) and (t). HeLa CCL2 (ATCC) cells were used in the remaining panels. Scale bars represent 10 μm .

Author Manuscript

Author Manuscript

Author Manuscript

Author Manuscript

Table 1

Physical and optical data.

Protein	Ref. ^a	λ_{ex} ^b	λ_{em} ^c	ϵ ^d	Φ^e	Brightness ^f	Photostability ^g	pK _a ^h	Maturation ⁱ
LanYFP	^j	513	524	150	0.95	424	ND	3.5	ND
dLanYFP	^j	513	524	125	0.90	335	ND	ND	ND
mNeonGreen	^j	506	517	116 ± 4	0.80 ± 0.016	276	158 ± 13	5.7	< 10
Clover	7	505	515	111	0.76	251	50	6.2	30
YPet	2	517	530	104	0.77	238	49	5.6	ND
mCitrine	2	516	529	77	0.76	174	49	5.7	ND
mVenus	2	515	528	92	0.57	156	15	6.0	ND
EYFP	2	514	527	83	0.61	151	60	6.9	ND
mEmerald	2	487	509	57	0.68	116	101 ^j	6.0	ND
sfGFP	2	485	510	83	0.65	161	157 ^j	5.5	ND
mWasabi	15	493	509	70	0.80	167	93	6.5	ND
mAG	16	492	505	42	0.81	100	ND	6.2	ND
mEGFP	2	488	507	56	0.60	100	150 ^j	6.0	25 ^k

^jThis study; standard deviations (n = 4 for ϵ and (x003C6); n = 20 for photostability) shown for mNeonGreen data.^aSource of data unless otherwise noted.^bExcitation maximum in nm.^cEmission maximum in nm.^dExtinction coefficient in $\text{mM}^{-1}\text{cm}^{-1}$, determined by alkali denaturation method.^eFluorescence quantum yield.^fProduct of ϵ and (x003C6), expressed as a percentage of mEGFP brightness.^gTime in s to photobleach from 1000 to 500 photons per s per molecule in live cells under widefield arc-lamp illumination (see **Methods**).^hpH at which fluorescence intensity is 50% of its maximum value.ⁱTime in min for fluorescence to reach its half-maximal value after exposure to oxygen at 37 °C.

Author Manuscript

Author Manuscript

Author Manuscript

Author Manuscript

j Photostability measurements of Emerald and mEmerald have historically been difficult to replicate, especially using purified proteins, due to the presence of a fast initial photobleaching component g_1 , and so the additional *Aequorea*-derived GFPs, sfGFP and mEGFP, have been included for comparison. Note that in our hands, mEmerald performs substantially better as a fusion tag than sfGFP in most experiments.

k Data from ref. 7. ND = not determined.